Journal of
Advanced Manufacturing Science and Technology
jamst@jamstjournal.com;jamst2020@126.com
www.jamstjournal.com

Influence of tool corner radius on chip geometrical characteristics of machining Zr-based bulk metallic glass

Haidong YANG[a], Libao ZHANG[a], Haodong LI[a], Junsheng ZHANG[a,b,*], Huohong TANG[a,b], Shunhua CHEN [a,b,*]

[a] *School of Mechanical Engineering, Hefei University of Technology, Hefei 230009, China*
[b] *Key Laboratory of Advanced Functional Materials and Devices of Anhui Province, Hefei University of Technology, Hefei 230009, China*

Received 25 June 2024; revised 24 July 2024; accepted 2 September 2024; Available online 5 September 2024

Abstract: The effect of tool corner radius on the chip geometrical characteristics of low-speed cutting $Zr_{57}Cu_{20}Al_{10}Ni_8Ti_5$ bulk metallic glass (at%, noted as Zr57 BMG) were studied. Additionally, traditional industrial pure zirconium (Zr702), titanium alloy (TC4), and 45 steel were selected as comparative materials. Continuous ribbon-shaped chips were formed during the turning of Zr57 BMG. The observable burrs were the result of chip tearing and dropping off layer by layer along multiple scratches. Serrated chips with numerous secondary shear bands (SSBs) were generated during the machining of Zr57 BMG. As the corner radius increased from 0.4 to 1.6 mm, the serration pitch P decreased from 29.68 to 6.2 μm, showing an increase in serrated frequency. Besides, the formation of BMG chips is associated with multiple shear behaviors. The stability of the serrated chip formation was quantitatively analyzed using three-parameter Weibull statistical analysis. Generally, the Weibull modulus of the inclination angles for serrated chips increased with the increase of corner radius, indicating that the chip formation process was more stable, which was conducive to superior machined surface quality. The machined surface roughness Ra decreased from 0.5 to 0.23 μm, which was consistent with the Weibull results. This work is of significant importance for understanding the state of the machining process from the perspective of chip characteristics.

Keywords: Bulk metallic glass; Machining; Chip formation; Corner radius; Statistical analysis

1. Introduction

Bulk metallic glasses (BMGs) were named for the lack of a crystalline structure which conventional metals possessed and their properties were similar to those of glass[1]. In contrast to traditional alloy materials, BMGs exhibited a unique arrangement characterized by short-range order and long-range disorder at the atomic level[2]. This structure led to the absence of structural defects such as grain boundaries and dislocations, resulting in their exceptional mechanical properties and processing characteristics[3]. The exceptional properties of BMGs had rapidly positioned them as a new class of materials, showing great application potential in various fields including national defense equipment, precision machinery[4], electronic information, and chemical engineering[5].

To facilitate their broader application, it was essential to conduct thorough researches on the machining of BMGs. This included optimizing cutting tools, developing suitable machining parameters, and revealing chip formation mechanisms. Due to their distinct atomic structure compared to traditional alloys, BMGs exhibited different cutting characteristics. Despite their high hardness and strength, the cutting forces of BMGs were lower than those of traditional alloys[6]. Although BMGs were brittle at room temperature, the chips produced during machining were serrated ribbon-shaped, which may be related to their low thermal conductivity[7]. Bakkal et al.[8] found that severe drill wear during the drilling of BMGs would cause the generation of chip light emission. It was observed that during the grinding of BMGs, a lower feed rate tended to result in surface crystallization more readily than a higher feed rate, which was likely due to the longer contact time between the grinding wheel and the workpiece at lower feed rates[9]. Yang et al.[10] conducted experiments on high-speed turning of Zr-based BMGs and observed that oxidation reactions occurred on the chip surface, which were progressively covered by powder particles.

Chip morphology reflects the state of cutting process, and the chip formation process will influence the cutting characteristics, including cutting force, cutting heat, tool wear, and surface quality. Early research showed that serrated chips, with adiabatic shear bands, was found during low-speed cutting BMGs, similar to titanium alloys and austenitic stainless steels[11]. The degree of chip defor-

* Corresponding author. *E-mail address:* zhangjunsheng90@126.com (Junsheng ZHANG), shchen@hfut.edu.cn (Shunhua CHEN)
Peer review under responsibility of Editorial Committee of JAMST
DOI: 10.51393/j.jamst.2025012

mation, induced by temperature, varied with the increase of cutting speed. When the cutting speed exceeded a certain threshold value, the outer layer of chips oxidized and released heat, resulting in interior crystallization. Chen et al.[7] compared the chip morphology of Zr-based BMG with that of Zr-based BMG composite (BMGC), Zr702, TC4, and 45 steel, and observed distinct shear bands characterizing the plastic deformation on the back surfaces of BMG chips. Chau et al.[12] conducted orthogonal cutting experiments on BMG to elucidate the mechanism of shear band formation and propagation, and investigated its impact on the quality of the machined surface. Kodama et al.[13] performed precision cutting experiments near the glass transition temperature and observed that the shear angle increased when the cutting speed was excessively high. In addition, Liu et al.[14] studied the influence of tool geometric parameters on the shape and morphology of Zr-based BMG chips, and found that as the number of cutter edges increased, sawtooth spacing on the free surface increased, and the plastic flow was obviously enhanced.

In general, previous researches indicated that the morphology of BMG chips was mainly influenced by cutting parameters and tool geometric parameters. However, current research primarily focused on the influence of cutting parameters on chip morphology, and few studies were conducted on the effects of tool geometric parameters on chip morphology. Particularly the corner radius showed a significant influence on chip morphology. Consequently, the influence of corner radius on the chip characteristics of machining Zr-based BMGs was investigated in this work. Additionally, to study the relationship between machined surface quality and chip morphology, a quantitative analysis on the stability of the serrated chip formation was conducted. The research results would provide guidance for the selection of tool geometric parameters to achieve superior surface quality and enhance the engineering applications of BMG materials.

2. Experimental

2.1. Workpiece materials

The experimental material employed in this study was $Zr_{57}Cu_{20}Al_{10}Ni_8Ti_5$ BMG (at%, noted as Zr57 BMG), which was prepared using an arc melting furnace. The BMG rod had a diameter of 5mm and a length of 9mm. In order to elucidate the impact of amorphous structure on chip formation, crystalline alloys such as Zr702, TC4, and 45 steel were selected as comparative materials due to the shared primary element with Zr-based BMGs, comparable mechanical properties to Zr-based BMGs, and widespread application, respectively. Their mechanical and physical properties are listed in Table 1.

2.2. Experimental set-up

The turning experiment was conducted on a CA6140 lathe equipped with a Kistler 9257B three-axis dynamometer, as shown in Fig. 1. The cutting parameters were kept constant, with a cutting speed of 0.16 m/min, feed rate of 0.039 mm/r, and cutting depth of 0.2 mm. The tool utilized in the cutting experiment was a polycrystalline cubic boron nitride (PCBN) tool with a CBN content of 85%. The tool was sharpened using a specialized tool grinding machine, the ZT-90, to achieve various tool geometric parameters. In order to ensure the reliability of experimental results, each cutting condition was repeated for three times during the cutting process. To investigate the effect of corner radius on the chip formation of Zr57 BMG, the tool rake angle, orthogonal clearance angle, and entering angle were kept constant as 0°, 7° and 90° respectively. The tool corner radius varied from 0.4 mm, 0.8 mm, 1.2 mm to 1.6 mm. After the turning, the average surface roughness (Ra) of the machined surfaces was measured using a profilometer (JH-340). The JSM-6490LV scanning electron microscope (SEM) was used to examine the morphology of the chips.

3. Chip morphology and geometric features

3.1. Chip shape and back surface morphology

During machining, the formation of chips affected the stability of cutting process, and the chip morphology can provide valuable information about cutting operations. To investigate the effect of corner radius on the chip formation of Zr57 BMG, the chip morphologies were detailly inspected using SEM. Fig. 2 showed the shape and back surface of BMG chips, obtained by cutting with various corner radii. The continuous spiral chips were observed under all kinds investigated conditions, and the chip shape became more regularly curled as the corner radius increased. According to the curling shapes of the chip, when the corner radius is less than or equal to 1.2 mm, the chip shapes exhibited a cross-curling in the direction of width[15]. Conversely, for the corner radius of 1.6 mm, the chip shapes presented an upwards-curling that generated along the thickness direction. The chip shape indicated that the BMG material was removed in a ductile-removing mode, despite its brittleness at room temperature. Chips with a higher curl degree could be in a better state for chip flow, because they were less prone to get entangled on the workpiece, that might deteriorate the machined surface quality and cause safety issues. Since the test tools lacked a chip breaker and were thus not conducive to chip breaking, continuous chips tended to generate regardless of tool parameters. The chip breakage can deteriorate surface roughness. Hence the stable continuous chip flow state might be the reason for the superior surface quality of Zr57 BMG machining. The change in the curling degree of chips was the result of complex thermomechanical coupling phenomena. High cutting forces generated when increasing the corner radius. And, concurrently, a substantial amount of cutting heat was generated and accumulated, owing to the limited thermal conductivity of BMG, which softened the removed material and ultimately promoted chip curling.

The newly generated surface of chips looked smooth and shiny. However, closer inspection in magnified images revealed that there were microparticle deposits, scale-like patterns, scratches, burrs, cracks, and shear bands on the surface. Here, the chip surface interacted with the microchipping protrusions on the cutting edge on the

Table 1 Mechanical and physical properties of the experimental materials.

Materials	Yield strength (MPa)	Hardness (HV)	Melting point (°C)	Thermal conductivity (W/m·K)
Zr57 BMG	1635	537.3	822	7.1
Zr702	205	189.9	1852	22.0
TC4	862	305.7	1688	7.9
45 steel	450	282.5	1495	50.2

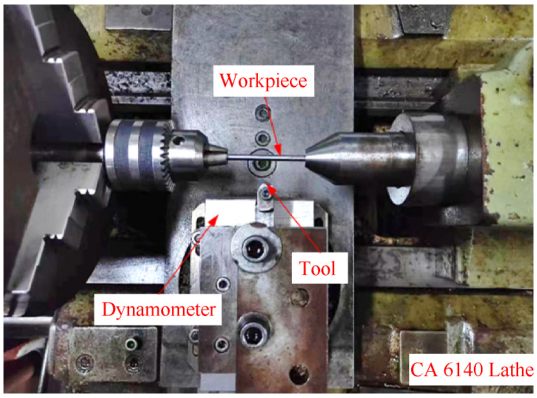

Fig. 1 Experimental setup for cutting test.

rake face, and was scraped along the chip flow direction under the applied cutting force, forming scratches on the newly generated surface of the chip. The appearance of microparticle deposits and scale-like patterns was attributed to the adhesion of chip fragments and plastic flow, which are caused by elevated temperatures due to cutting heat.

Further examination of the chip topography revealed that the burr formation differed significantly when cutting with different corner radii. Firstly, the burrs were formed at the outer edge of the curled chip with a corner radius of 0.4 mm, and at the inner edge of the curled chip with corner radii of 0.8 mm and 1.2 mm. And there was no detectable burr formation when a corner radius of 1.6 mm was used, as shown in Fig. 2. Secondly, the high magnification images in Fig. 2(c), 2(f) further revealed that the burrs, formed with a corner radius of 0.4 mm, resembled protrusions at chip edge, whereas the burrs formed with a corner radius of 0.8 mm and 1.2 mm resembled chip edge tearing, and were accompanied by cracks and multiple shear bands. Fig. 3 showed the schematic model of the undeformed section of chip, which resembled a comma with uneven thickness, owing to the employment of a round-nosed tool. In order to facilitate the following discussion, the two sides of the un-

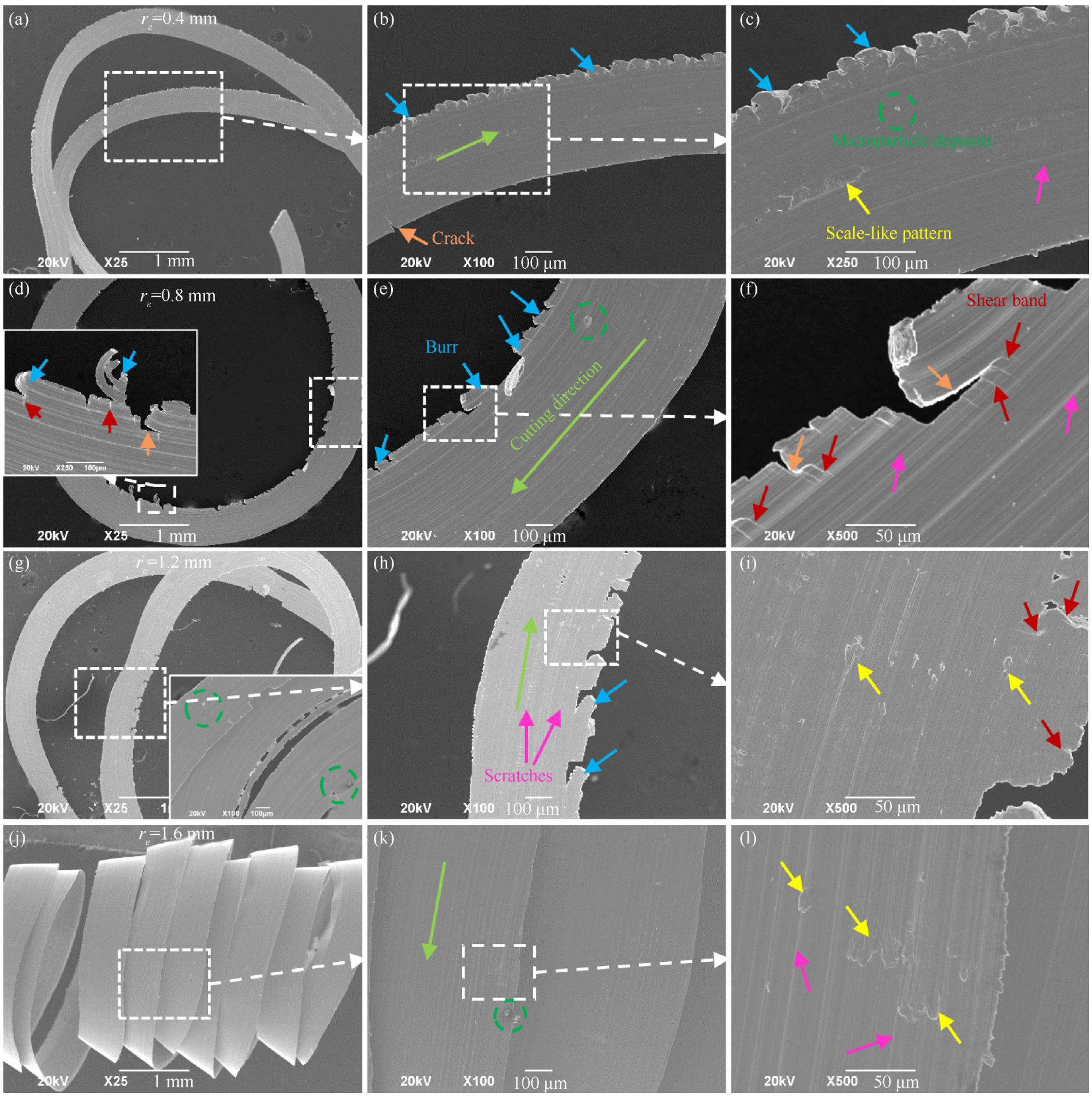

Fig. 2 SEM images showing shapes and back surfaces of Zr57 BMG chips at corner radius of 0.4 mm (a-c), 0.8 mm (d-f), 1.2 mm (g-i) and 1.6 mm (j-l), respectively.

deformed section of chip were marked as I and II respectively, with II being thicker than I, as illustrated in Fig. 3. The chips curled when separated from the workpiece. The inner edge of the curled chip corresponded to the side I of the undeformed section of chip. The uncut chip thickness, produced by corner radius of 0.4 mm, was larger than the other three test parameters, especially on the side II (see details in section 3.3). The material in the cutting zone undergone severe shearing and extrusion deformations during cutting. As a result of thermal softening effect, the amorphous material, that had been plastically modified, became more fluid. When the volume of material engaged in the extrusion rose, the material may overflow under the extruding effect of the tool, resulting in this protrusion-like burr at a 0.4 mm corner radius. On the other hand, for the burrs generated in cutting with corner radii of 0.8 mm and 1.2 mm, shear bands were distributed on one side of the crack like tributaries, and expanded into the interior of the chip, as shown in Fig. 2(f). The shear band, which was considered to characterize the plastic deformation of BMGs, resulted from activation and coordinated rearrangement of the microscopic plastic regions noted as shear transformation zones (STZs). When stress was over the yield stress, shear bands initiated at the stress concentrator and propagated outward. And cracks generated by further expansion of shear bands. The scratches, which functioned as stress concentrators, were the origins of shear bands and cracks, as seen in Fig. 2(f). The cracks propagated along the scratches, tearing the chips and finally forming the tear-type burrs. The magnified view in Fig. 2(g) showed that a whole piece inside the curled chip was about to fall off along the scratches. Moreover, the close-up in Fig. 2(d) captured the phenomenon of burrs generated along scratches of different chip widths, demonstrating that the observable burrs were the result of chip tearing and dropping off layer by layer along multiple scratches.

With the increase in corner radius, more scale-like patterns were observed on the chip surfaces. This could be attributed to the fact that as the corner radius increased, more cutting heat was generated, which led to a decrease in material viscosity and intensified the plastic flow on the chip surface.

In order to further study the law of burr formation, b_{ch} which represented the maximum chip width in the vicinity of the burr-free zone and b_{ch}^* which indicated the reduced chip width due to the tearing effect of the burr were measured on the back surface of chips, as shown in Fig. 4. Here, the maximum chip width was measured by carefully identifying the maximum width part of chips in a cut using SEM to minimize inaccuracies, which were caused by the inner edge detaching of chip (if burrs appeared, take the part with

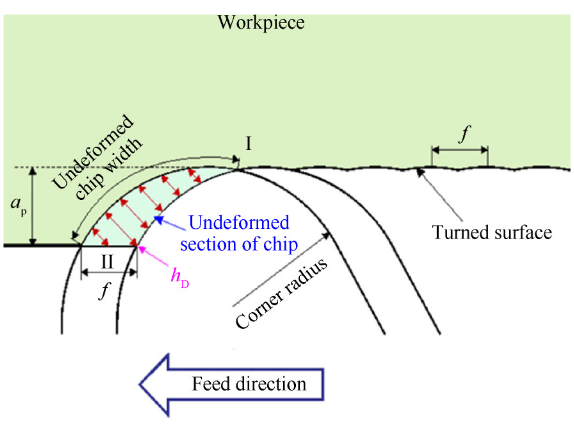

Fig. 3 Description of cross section of undeformed chip during turning.

burrs). Fig. 5 showed the results of measured chip width, which increased as the corner radius increased. Theoretically, the undeformed chip width b_D can be estimated as[16]

$$b_D = r_\varepsilon\left(\kappa_r + \arcsin\left(\frac{f}{2r_\varepsilon}\right)\right) + \left(a_p - r_\varepsilon(1-\cos\kappa_r)\right) \times \sin\kappa_r \quad (1)$$

where b_D was the undeformed chip width, r_ε was the tool corner radius, κ_r was the entering angle, f was the feeding rate, and a_p was the cutting depth.

Given other parameters, the undeformed chip width at different corner radii were calculated and illustrated in Fig. 5. The undeformed chip width increased as the corner radius increased. The actual chip width was smaller than the undeformed chip width, indicating that the width deformation coefficient $\xi_b = b_D/b_{ch}$ always exceeded 1. For the tear-type burrs formed with corner radii of 0.8 mm and 1.2 mm, the position of burr forming can be expressed by the ratio ε:

$$\varepsilon_{0.8} = b_{ch}^*/b_{ch} \approx 0.90 \quad (2)$$

$$\varepsilon_{1.2} = b_{ch}^*/b_{ch} \approx 0.87 \quad (3)$$

The results indicated that the origin of these tear-type burrs was nearly identical position. As shown in Fig. 3, the undeformed chip thickness increased gradually from side I to side II. Chips near side I were too thin, and were easily broken and torn, when subjected to cutting stress in the direction of chip thickness, resulting in such tear-type burrs. The cut-off position for the tearing phenomenon was where the chip thickness was large enough to resist stress failure. When cutting with a corner radius of 0.4 mm, the cutting stress was insufficient to cause this tearing phenomenon at the thin edge of chips, due to the thicker undeformed section. However, tear-type burrs were not observed despite the smaller undeformed chip thickness and larger cutting forces, produced by a corner radius of 1.6 mm. This may be due to that the curvature of tool cutting edge decreased as the corner radius increased, thus reducing the degree of stress concentration. The burr formation can also be altered by adjusting the feed rate, given that it also had a considerable impact on the undeformed chip thickness. Studies had shown that burrs, formed on thin edges, affected the machined surface roughness. Thus, minimizing burr formation can be a reliable approach to optimize the cutting process of BMGs.

The chip morphology of four workpiece materials was characterized at α_n=7°, r_ε=0.8 mm and κ_r=90°, and the SEM images of the chip shape and back surface are shown in Fig. 6. Under the current parameters, continuous spiral chips of typical ductility material cutting formed in all four materials, with upward-curling chip shapes for 45 steel and Zr 702, and cross-curling chip shapes for BMG and TC4. Due to the low plasticity of BMG, chips were less curled than those of the other three materials. Microparticle deposits and scratches were presented on the chip back surface of each material. Due to the distinctive deformation mechanisms between amorphous and traditional crystalline alloys, shear bands that usually appear in BMG chips, were not found on the back surface of these comparison material chips. It was observed that the chip edge tearing phenomenon occurred in the chip formation of each material, but the size and quantity of chip burrs were significantly different. Large burrs could be seen at the thinner edges of Zr57 BMG and TC4 chips, while the burrs of Zr702 and 45 steel chips were small. This could be attributed to the low strength and high plasticity of Zr702 and 45 steel. Moreover, Fig. 7 showed the chip width bch and width deformation coefficient ξ_b of the four materials. The dotted line represents the undeformed chip width under the current cutting parameter. The chip width of Zr57 BMG chip was found to be

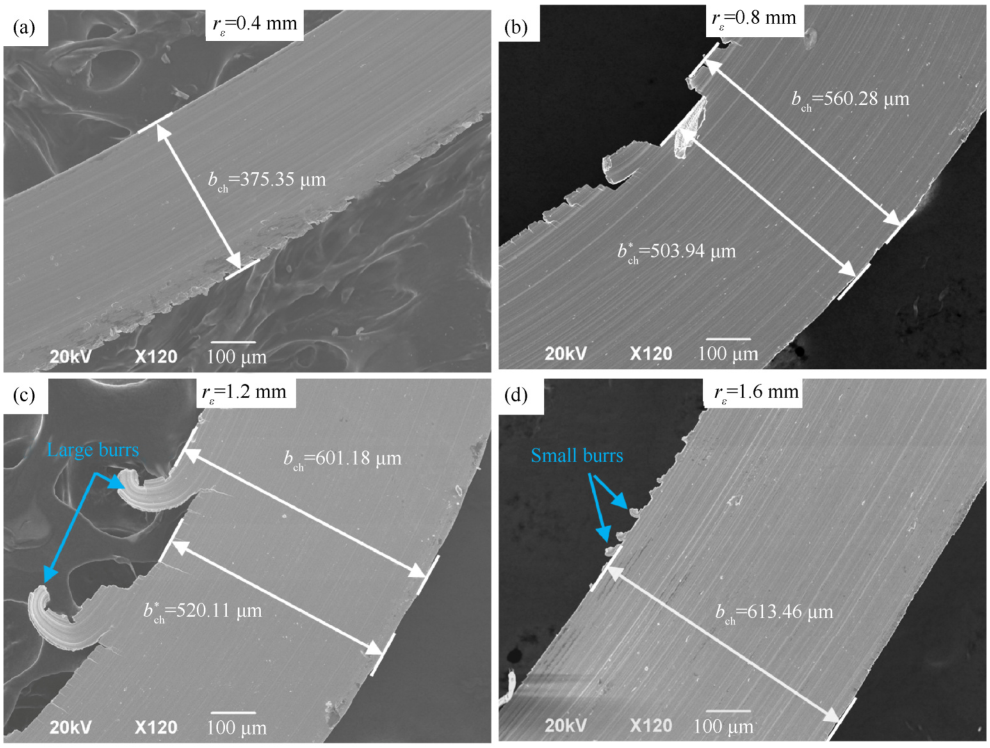

Fig. 4 Sketch showinge measurement of chip width at the corner radius of 0.4 mm (a), 0.8 mm (b), 1.2 mm (c) and 1.6mm (d), respectively.

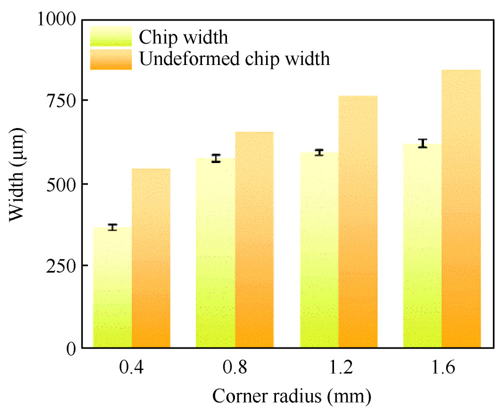

Fig. 5 Chip width and undeformed chip width of Zr57 BMG at different corner radii.

the largest one, followed by the TC4 chip, the Zr702 chip, and the 45 steel chip. The variation trend of width deformation coefficient was opposite to that of the chip width, and the value of ξ_b was related to the plasticity of the material. Zr57 BMG had the smallest deformation coefficient due to its lowest plasticity.

3.2. Serrated chip morphology

Fig. 8 showed the typical serrated chip morphology of Zr57 BMG at a corner radius of 0.4 mm, including the free surface, inner side surface, and outer side surface of the chip. The individual serrated section of the serrated chips was arranged almost parallel, at a certain inclination angle, and at a nearly constant interval on the micrometer scale along the cutting direction. Adjacent serrated sections were separated by a distinct fracture, with the intermediate narrow region being the primary shear zones (PSZs)[17]. Due to the inward curling of the chips, the serration spacing decreased significantly from the outer side to the inner side in the width direction, making the inner serrations appear more packed. The regular serrated structure was ascribed to the periodic shear-banding formation induced by strain localization in the PSZs, which originated at the tool-chip interface and propagated to free surface[18]. Given that the serrations at the inner side surface were much higher than those at the outer side surface, it was evident that the inner and outer side surfaces corresponded to the side I and II of the undeformed chip (Fig. 3), respectively. Despite this, it was found that the height of an individual lamellar structure experienced several significant fluctuations in the width direction of the chip, causing the free surface appearing to be constituted of groove-like and ridge-like strips along the cutting direction. This differed from its uniform transition thickness on the undeformed section of chip, which may be the result of tool wear and the built-up edge attached to the cutting edge as stress concentration zones. That affected the stress distribution along the cutting edge of the tool, causing varying degrees of shear band slip and chip deformation. Furthermore, sparse secondary shear bands (SSBs) were visible within the serrated sections, indicating that severe plastic deformation was highly localized within the individual chip section. Within each serrated section, the SSBs extended in almost the same direction, initiating from the high strain region and progressing to the low strain region[19]. It had been reported that the formation of SSBs within the individual serrated sections, during the generation of BMGs chips, was actually an intrinsic mechanism of the material for enhancing plastic deformation capability in order to prevent rapid shear and catastrophic fracture along a single shear plane[17].

The outer side surface and the free surface morphology of Zr57 BMG chips, with corner radii varying from 0.4 mm to 1.6 mm, are presented in Fig. 9 and Fig. 10, respectively. Obviously, increasing the corner radius reduced the height of serrated sections and the serration pitch P between two consecutive serrated sections, and altered the inclination angle of the shear plane. The laminar structure in the free surface was also denser. Furthermore, it was observed that the morphology of individual chip sections was profoundly af-

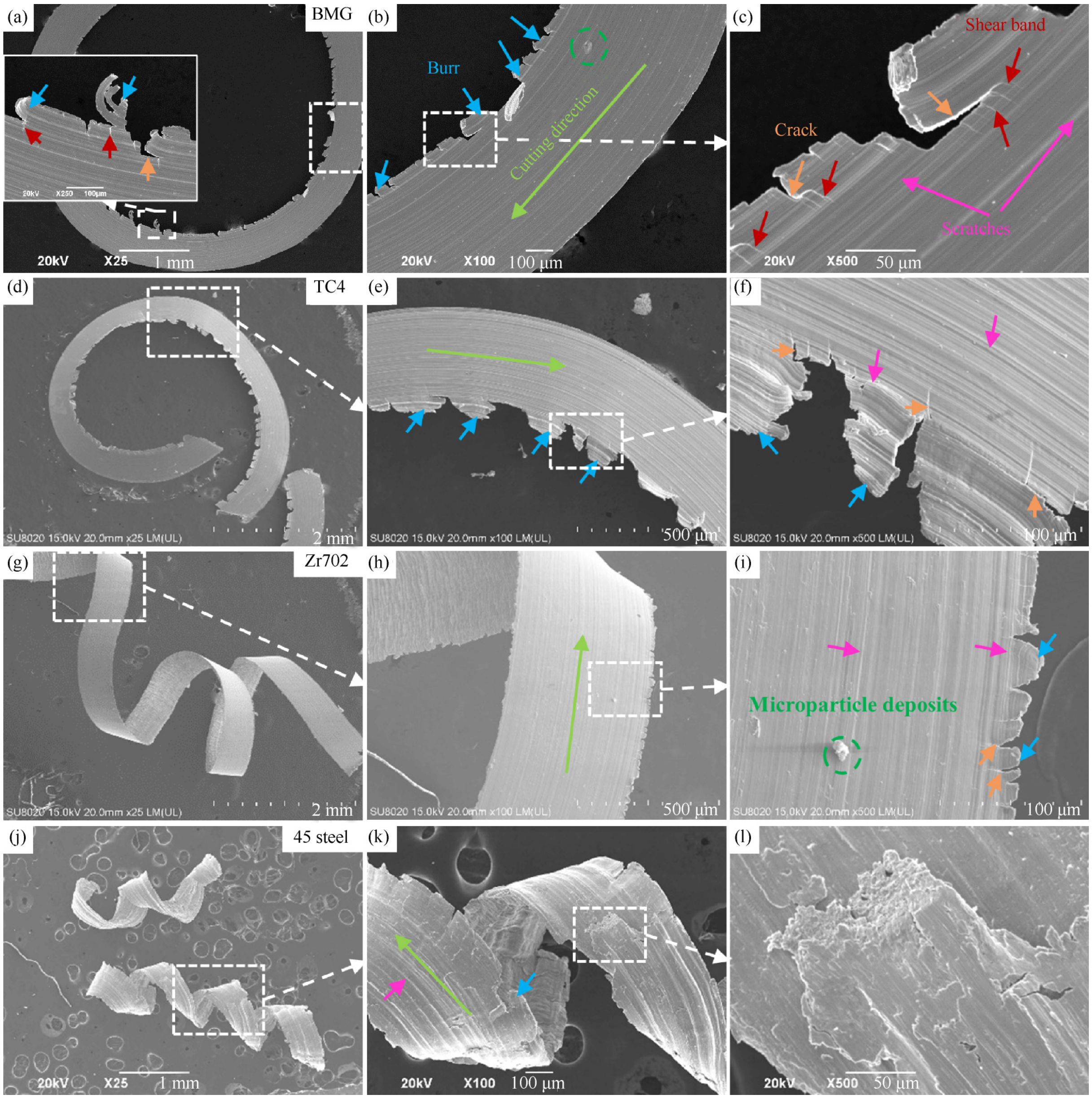

Fig. 6 SEM images showing shapes and back surfaces of chips for different workpiece materials at a corner radius of 0.8 mm, an orthogonal clearance of 7°, and an entering angle of 90°: BMG (a-c), TC4 (d-f), Zr702 (g-i), and 45 steel (j-l).

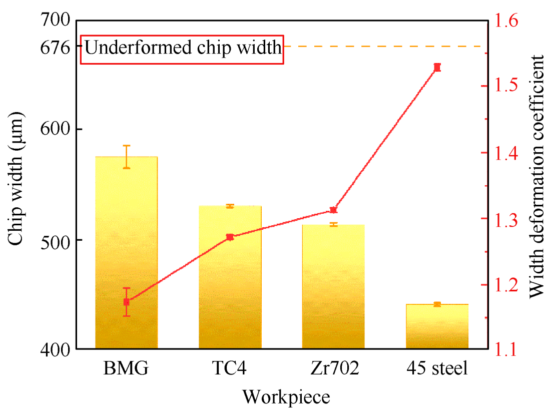

Fig. 7 Chip width and width deformation coefficient of the four workpiece materials.

fected by increasing corner radius. At a corner radius of 0.4 mm, as shown in Fig. 4(b), some radiating ridges were clearly apparent on the fractured PSZs of the serrated section, which were typical BMG fracture surface features related to the degree of plastic deformation. As the corner radius increased to 0.8 mm, the number of SSBs within each chip section increased dramatically due to severe plastic deformation, which caused the emergence of numerous fish-scale-like flake features along the SSBs. Furthermore, a small serrated section emerged alongside the larger one at the chip root. This phenomenon was referred as "twinned shear" and was previously reported to occur in ultra-precision micro-cutting (UPMC) of BMGs[20]. According to the reports, a twinned minor shear existed in the cycle of each serrated section formation, which occurred after the shear fracture of PSZs, and further split the serrated section in the form of a second shearing, producing a smaller serrated shape following the larger one. Upon increasing the corner radius to 1.2 mm and then to 1.6 mm (Figs. 4(f), 4(h)), it was found that the minor shear effect was significantly enhanced, and even multiple small serrated sections were formed alongside the large serrated section, especially when the corner radius was 1.6 mm. This indi-

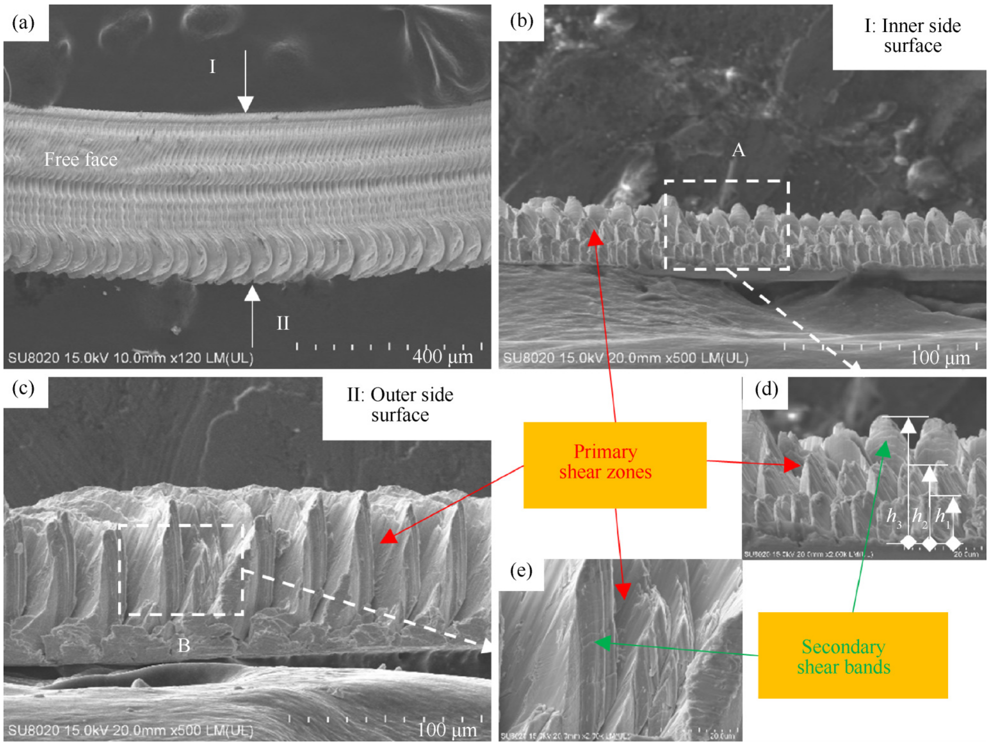

Fig. 8 SEM images showing typic serrated chip morphology of Zr57 BMG at a corner radius of 0.4 mm. (a) Free surface morphology of chip, (b) I-side view of chip showing medial surface, (c) II-side view of chip showing extracellular surface, (d) Details corresponding to square "A" in (b), and (e) details corresponding to square "B" in (c).

cated that a multi-step shear event may occur in the formation of each individual serrated section of BMGs chips. Due to severe localized plastic deformation, during the cutting with large corner radii, multiple shear bands similar to the twinned shear bands generated in the individual serrated section, which originated from the chip root and split the serrated section into numerous small serrated sections after the shear fracture of PSZs. The finding suggests that the formation of BMG chips is associated with multiple shear behaviors, including shearing in the PSZs, multi-step shearing after the PSZs fracture, and secondary shearing within the individual serrated sections. These shearing behaviors may be progressively induced and intensified as increasingly severe deformation behaviors emerge.

As shown in Fig. 11, the side morphology of chips showed that Zr57 BMG, TC4, and Zr702 had serrated chips, where Zr57 BMG and TC4 chips exhibited more regular serrations in both form and frequency. However, the shape and geometry of each individual serrated section among Zr702 chips were significantly different and irregular. Compared to the serrated chips of TC4 and Zr702 under the same cutting condition, the serrated areas of the BMG chips had sharper edges and seemed to be more fragile. This was caused by the low plasticity of BMG, which implied that both brittle and ductile types of fracture were involved in the chip removal process. Low-speed cuttings of 45 steel produced continuous chips with multiple sheet layer units slipping along the shear plane and stacking. Although the serrated structure was difficult to detect, the PSZs between the shear layers were clearly visible on the free surface (Fig. 11(d)). However, it should also be noted that the generation and propagation of SSBs within the individual serrated structure was not seen in chips produced by machining crystalline alloys. The formation of serrated chips during BMG machining was phenomenologically very similar to that of crystalline alloys. Both types of serrations derived from the instability of laminar plastic flow caused by strain localization. In amorphous alloys, this localized plasticity was characterized by shear bands. But in nanocrystalline materials, dislocations due to grain boundaries and other imperfections played this function[21]. The investigation in chip morphology indicated that the chip formation mechanism was mainly attributed to inherent material properties.

3.3. Geometry of the chip

The chip shapes at different corner radii were investigated using SEM. Based on the outer side surface morphology of the serrated chip in Fig. 9, the maximum thickness of the serrated chip h_{max}, the thickness of the serrated chip in the continuous section h_{min}, the serration pitch P and the inclination angle φ were measured. Measurements were made by the SEM images with the image-pro plus software, each group of data was the average value of at least 10 measurements along the entire length of the chip, and the measured results were showed in Table 2.

According to Table 2, the maximum thickness of the serrated chip and the thickness of serrated chip in the continuous section decreased as the corner radius increased. From the values of h_{max} and h_{min}, the equivalent chip thickness h_{ch} of the serrated chip was expressed as[16]

$$h_{ch} = h_{min} + \left(h_{max} - h_{min}\right)/2 \tag{4}$$

Fig. 12 showed that the equivalent chip thickness decreased as the corner radius increased based on Eq. (4). For the current case of $f < \sqrt{2r_\varepsilon a_p - a_p^2}$, the maximum undeformed chip thickness h_D (see Fig. 3) can be calculated by Chen et al.[22], which was used to characterize the undeformed chip thickness:

$$h_D = r_\varepsilon - \sqrt{r_\varepsilon^2 + f^2 - 2f\sqrt{2r_\varepsilon a_p - a_p^2}} \tag{5}$$

The variation in undeformed chip thickness at different corner ra-

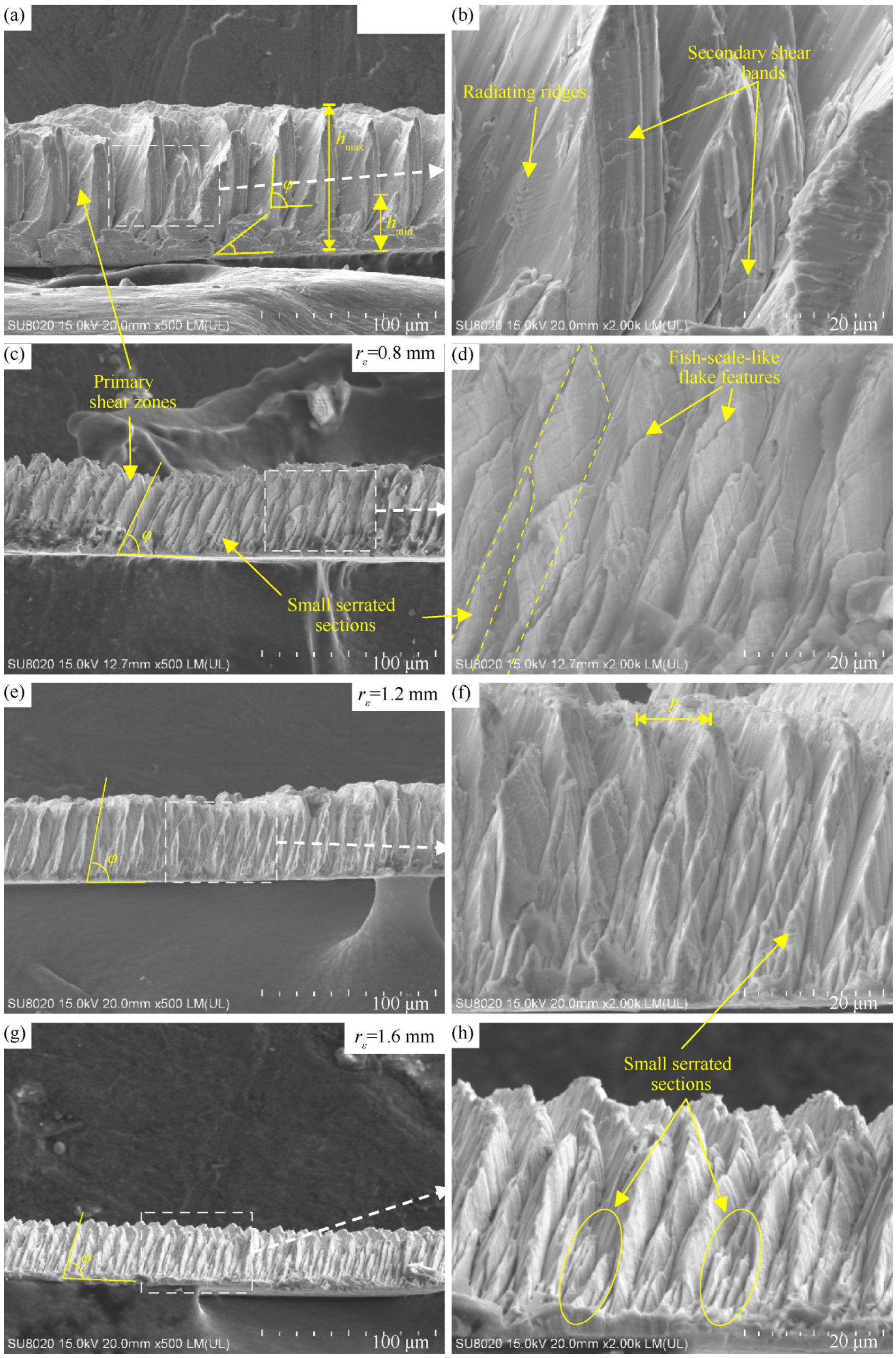

Fig. 9 SEM images showing side morphology of Zr57 BMG chips at corner radius of 0.4 mm (a-b), 0.8mm (c-d), 1.2 mm (e-f) and 1.6 mm (g-h), respectively.

dii was illustrated in Fig. 12. The undeformed chip thickness decreased as the corner radius increased. And the actual chip thickness was larger than the undeformed chip thickness, indicating that the thickness deformation coefficient $\xi_h = h_{ch}/h_D$ always exceeded 1.

The geometric characteristics of serrated chips were expressed as the serrated degree G_s and serrated frequency f_{chip}. The serrated degree G_s was evaluated by Dhale et al.[19]:

$$G_s = \left(h_{max} - h_{min}\right)/h_{max} \tag{6}$$

Fig. 13 showed the variation of the serrated degree of chips at different corner radii based on Eq. (6). The serrated degree had negatively correlation with corner radius. The asymptotic value of 1 indicated that the chip morphology was more discontinuous, i.e, the more prominent the serrations. This result indicated that the deformation degree of individual shear bands increased in the PSZs, and the level of separation between chip elements rose as the corner radius decreased.

The chip serrated frequency within the regime of low-speed cutting of BMG was an important indicator to characterize the serrated chips. The occurrence frequency of serrated elements was distinct at different corner radii. Hence, the serrated frequency may be used

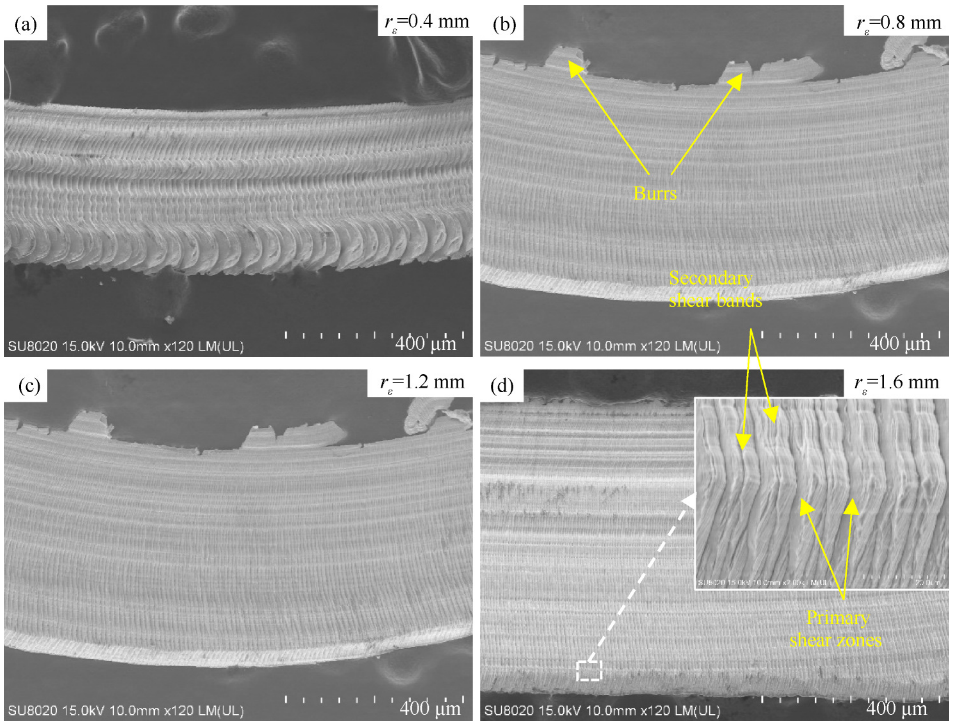

Fig. 10 SEM images showing free surface morphology of Zr57 BMG chips at corner radii of 0.4 mm (a), 0.8 mm (b), 1.2 mm (c), and 1.6 mm (d), with a magnified image showing details of lamellar structures in (d).

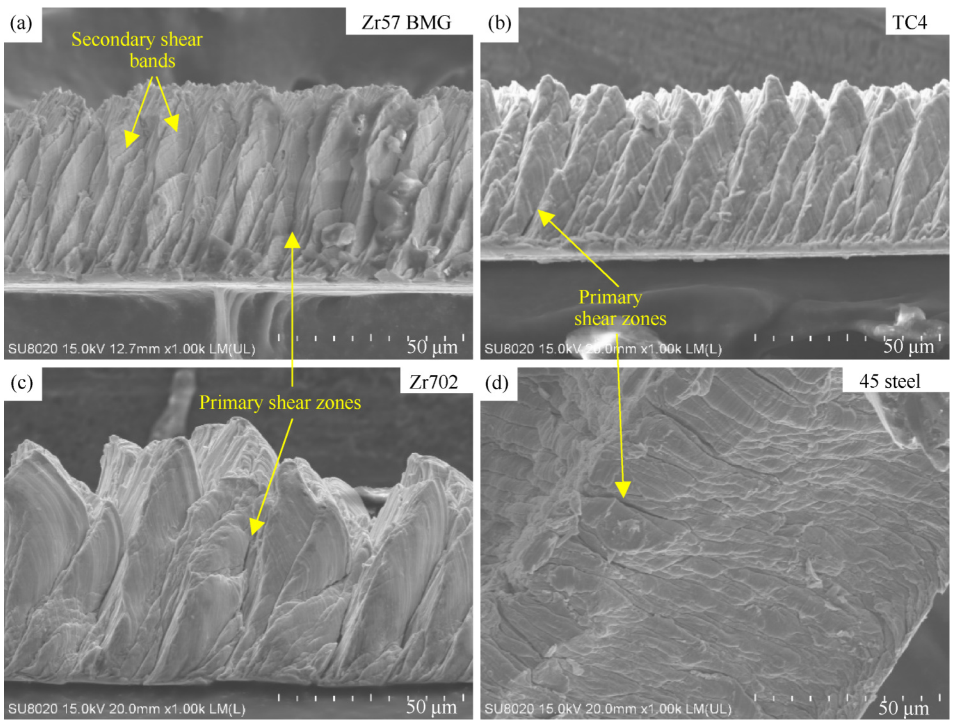

Fig. 11 SEM images showing side morphology of chips for Zr57 BMG (a), TC4 (b), and Zr702 (c), and free surface morphology of chip for 45 steel (d).

Table 2 Measured geometric values of serrated chips of Zr57 BMG.

r_ε(mm)	h_{max}(μm)	h_{min}(μm)	P(μm)	φ(°)
0.4	78.81±4.91	32.56±2.89	29.68±5.44	79.36±5.86
0.8	50.10±3.17	41.11±2.30	10.98±2.05	74.58±4.34
1.2	43.67±3.83	36.90±3.64	8.27±2.87	75.97±4.82
1.6	30.37±1.64	26.56±1.33	6.20±1.90	75.97±5.19

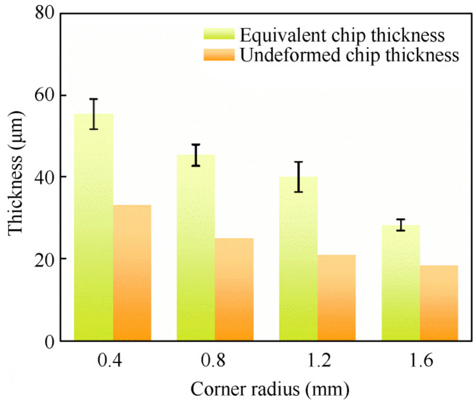

Fig. 12 Equivalent chip thickness and undeformed chip thickness at different corner radii.

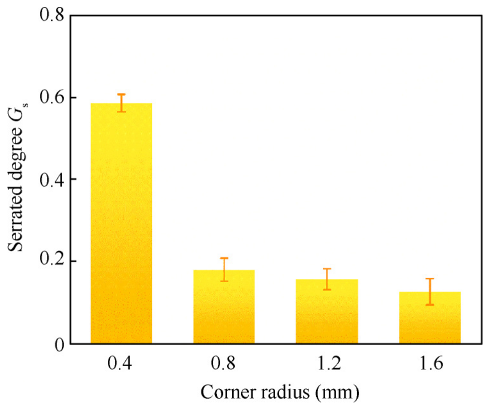

Fig. 13 Variation of serrated degree at different corner radii.

to represent variation. The frequency of the formation of serrated chip can be calculated by the formula[23]:

$$f_{\text{chip}} = \frac{v_{\text{chip}}}{p} = \frac{v_c h_D}{h_{\text{ch}} p} \tag{7}$$

where v_{chip} was the velocity of chips in the direction of tool rake face, v_c was the cutting speed, and p was the equivalent chip thickness pitch. The variation of chip serrated frequency at different corner radii, based on Eq. (7), was illustrated in Fig. 14. The parameter increased obviously with the corner radii, which demonstrated the formation of more shear bands and localized shearing during the chip-removal process, as also seen on the free surface in Fig. 10.

According to Table 2, the most noticeable was the jump in P between corner radii of 0.4 mm and 0.8 mm, which dropped dramatically from 29.68±5.44 μm to 10.98±2.55 μm. As evidently seen

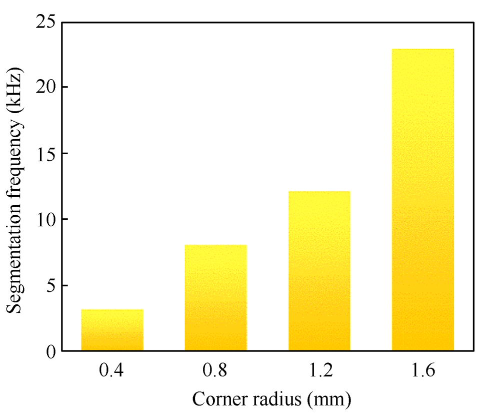

Fig. 14 Variation of serrated frequency at different corner radii.

from the side morphology in Fig. 9, adjacent serrated sections, formed at the corner radius of 0.4 mm, were separated farther apart, but those formed at the corner radius of 0.8 mm were nearly tight. This noticeable change was also reflected in the serrated inclination angle. As shown in Fig. 9(a), the shearing plane formed by a corner radius of 0.4 mm followed a curved path characterized by two strikingly distinct angles, with the inclination angle at the upper part of the chip φ being larger than the inclination angle (φ') at the bottom. Similar result was also found in Chen et al. 7, where cutting tests were performed at a corner radius of 0.4 mm. However, for larger corner radii ⩾ 0.8 mm, the shearing plane formed along a straight boundary with a well-defined inclination angle φ. Table 2 showed that the average values of the measured serrated inclination angle were about 79° at a corner radius of 0.4 mm (the inclination angle at the upper part of the chip), but the values remained around 75° in the other three cases. In previous molecular dynamics simulations, a different mechanism of shear band propagation in PSZs with different cutting depths was revealed by Avila et al.[21]. According to the report, the deeper cuts resulted in shear bands with a large pitch, thicker widths, and a curved trajectory. The shear bands initially emerged with a smaller propagation angle from the tool edge, by propagation first towards the sample interior, and then propagated to the free surface with an increasing angle until it approached the angle of the PSZ. In the case of shallow cuts with a small shear band pitch, the shear bands propagated directly from the tool edge to the free surface with a fixed angle. The size of shear bands pitch was an essential feature that manifested chip deformation degree. In this investigation, a similar phenomenon of pitch change was also observed, but occurring at varying corner radii. Based on the results of this work and Avila et al.[21], it can be predicted a similar transition in the propagation behavior of shear bands as the corner radius increased from 0.4 mm to 0.8 mm. A possible explanation for the shear band transition behavior was the spillover effect induced when the shear band grew with the PSZs beyond its limit. In the case of cutting BMG with a small corner radius, plastic strain was highly localized in each individual shear band within PSZs, and shear bands can accomplish complex evolution and growth processes. This may be considered as a mature form of shearing. However, a larger corner radius tended to induce a larger cutting force and thus more severe plastic deformation, which resulted in more PSZs being activated and more shear bands generation. In this case, undeveloped shear bands within the PSZs tended to fracture catastrophically under excessive stress before they had even finished propagation.

For the machining of BMGs, the serrated chip formation was generally considered to be extremely periodic. However, according to Fig. 9 and the significant standard deviation of the values in Table 2, the geometric parameters of the serrated structure were not highly consistent in one cut. Despite the availability of extensive data on the serrated chip formation of machining BMGs, the stability of serration formation had been neglected. The analysis of the stability of serrated chip formation during machining can help better understand the chip formation mechanisms, predict and regulate the machining process, and thereby improve machining efficiency, accuracy, and reliability, which was of great significance. For this reason, the Weibull distribution was used to quantitatively analyze the stability of the serrated inclination angle at different corner radii, which was also one of the most popular models in the mainstream reliability community. The cumulation distribution function of the three-parameter Weibull distribution was given by Tang et al.[24]:

$$P = 1 - \exp\left[-\left(\frac{\varphi - \varphi_u}{\varphi_0}\right)^m\right] \tag{8}$$

where P was the probability for a given serrated inclination angle φ, φ_0 was the scale parameter, m was the Weibull modulus, and φ_u was the cut-off value. The Weibull modulus was a shape parameter of the density distributions, and a bigger m value signified a smaller dispersion of the data set. The value of m can be obtained by linearizing Eq. (8), as shown in the following expression:

$$\ln\left[-\ln(1-P)\right] = m\ln\left(\varphi - \varphi_u\right) - m\ln\left(\varphi_0\right) \tag{9}$$

A series of consecutive serrated inclination angles were measured for each condition. The resulting three-parameter Weibull plots of the serrated inclination angle at different corner radii were illustrated in Fig. 15, where the slope of the fitted line represented the Weibull modulus. It can be seen that the Weibull modulus generally increased with the increase of corner radius, demonstrating that the serrated inclination angles had high uniformity values at larger corner radii. The periodicity of the shear-band formation appeared to be more homogeneous at larger corner radii. It also indicated that the serrated flow formation was turned from an unstable state to a stable state as the corner radius increased. Chip formation was an important indicator for machined surface quality. According to the previous report, the superior cuttability of the BMGs may be attributable to their capacity to generate ideal serrated chips. In this case, the findings may provide support for this notion. As shown in Fig. 16, the surface roughness value of Zr57 BMG decreased with the increase of corner radius. The ideal serrated chip formation was conducive to a stable material removal process, suggesting that the cutting force was constant without readily chattering, the surface residual pits were minimized, and the material removal was more adequate, resulting in a superior machined surface quality. This could also be due to their better serration periodicity and reproducibility along the chip generation direction, as shown in Fig. 12.

The formation of serrated chips reflected the cutting performance of BMGs at varying corner radii. Different from the chips of traditional crystalline alloys, serrated chips with numerous SSBs generated in the cutting of Zr57 BMG. The variation of tool geometric parameters also influenced the chip morphology. As the corner radius increased, more shear bands developed, which were manifested by an increase in serrated frequency and more SSBs within individual serrated sections. The three-parameter Weibull distribution can be used to quantitatively analyze the stability of the serrated flows for the chips. With the increasing of corner radius, the

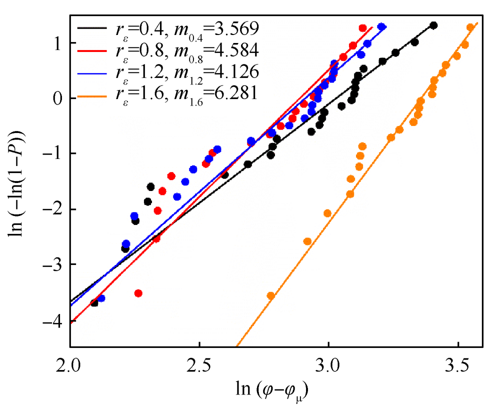

Fig. 15 Three-parameter Weibull plots for serrated inclination angles at different corner radii.

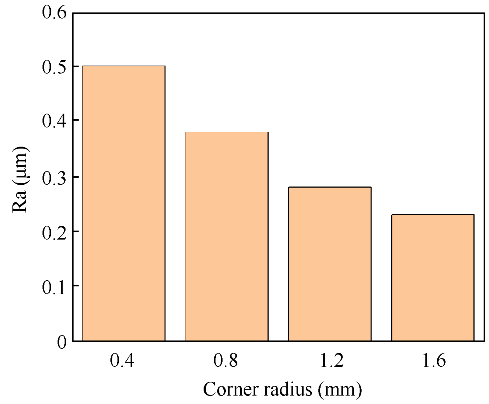

Fig. 16 Variation of surface roughness on change of corner radius.

Weibull modulus of the inclination angles for serrated chips also increased, which shown that the formation process of serrated chips changes from unstable to stable. The stable serrated chips are conducive to a better machined surface quality.

4. Conclusions

In this work, the effect of corner radius on the chip formation of Zr57 BMG was investigated. The shape and morphology of the chips in terms of chip shape, back surface morphology, and serrated chip morphology were analyzed. Then the three-parameter Weibull distribution was used to quantitatively analyze the stability of the chip serrated flows. The following conclusions can be drawn:

- Continuous ribbon-shaped chips were found during the turning of Zr57 BMG. Due to the low plasticity of BMG, chips were less curled than those of comparative materials. The observable burrs were the result of chip tearing and dropping off layer by layer along multiple scratches. And the burr formation differed significantly with different corner radii.
- As the corner radius increased, more shear bands developed, showing an increase in serrated frequency and more SSBs within individual serrated sections. The formation of BMG chips is associated with multiple shear behaviors, including shearing in the PSZs, multi-step shearing after the PSZs fracture, and secondary shearing within the individual serrated sections.
- The stability of the serrated chip formation can be expressed with three-parameter Weibull modulus. The Weibull modulus of inclination angles for serrated chips increased with the increase of corner radius, indicating the transition of the serrated chip formation from unstable to stable, which was conducive to the formation of better machined surface.

Acknowledgements

This work was mainly supported by the Fundamental Research Funds for the Central Universities of China (Grant no. PA2024GDSK0060; PA2023GDSK0075) and the Ningbo Science and Technology Innovation 2025 Major Project (Grant no. 2022Z047).

References

1. Khan MM, Nemati A, Rahman ZU, et al. Recent advancements in bulk metallic glasses and their applications: a review. *Critical Reviews in Solid State and Materials Sciences* 2018; 43(3): 233-268.
2. Axinte E. Metallic glasses from "alchemy" to pure science: Present and future of design, processing and applications of glassy metals. *Materials & Design* 2012; 35: 518-556.
3. Yavari AR, Lewandowski JJ, Eckert J. Mechanical properties of bulk

metallic glasses. *MRS Bulletin* 2007; 32(8): 635-638.
4. Inoue A, Takeuchi A. Recent development and application products of bulk glassy alloys. *Acta Materialia* 2011; 59(6): 2243-2267.
5. Chen SH, Cheng HY, Chan KC, et al. Metallic glass structures for mechanical-energy-dissipation purpose: A Review. *Metals* 2018; 8(9):689.
6. Bakkal M, Shih AJ, Scattergood RO. Chip formation, cutting forces, and tool wear in turning of Zr-based bulk metallic glass. *International Journal of Machine Tools and Manufacture* 2004; 44(9): 915-925.
7. Chen SH, Ge Q, Zhang JS, et al. Low-speed machining of a Zr-based bulk metallic glass. *Journal of Manufacturing Processes* 2021; 72: 565-581.
8. Bakkal M, Shih AJ, Mcspadden SB, et al. Thrust force, torque, and tool wear in drilling the bulk metallic glass. *International Journal of Machine Tools and Manufacture* 2005; 45(7-8): 863-872.
9. Bakkal M, Serbest E, Karipçin İ, et al. An experimental study on grinding of Zr-based bulk metallic glass. *Advances in Manufacturing* 2015; 3(4): 282-291.
10. Yang H, Wu Y, Zhang J, et al. Study on the cutting characteristics of high-speed machining Zr-based bulk metallic glass. *The International Journal of Advanced Manufacturing Technology* 2022; 119(5-6): 3533-3544.
11. Bakkal M, Shih AJ, Scattergood RO, et al. Machining of a Zr-Ti-Al-Cu-Ni metallic glass. *Scripta Materialia* 2004; 50(5): 583-588.
12. Chau SY, To S, Wang H, et al. Effect of cutting speed on surface integrity and chip formation in micro-cutting of Zr-based bulk metallic glass. *The International Journal of Advanced Manufacturing Technology* 2021; 114(11-12): 3301-3310.
13. Kodama H, Okuda K, Inada T. Chip formation during precision cutting of metallic glass. *Advanced Materials Research* 2016; 1136: 265-270.
14. Liu Y, Gong Y, Liu W, et al. Effect of milling parameters on chip shape and chip morphology for Zr-based bulk metallic glass by using micro-groove milling. *The International Journal of Advanced Manufacturing Technology* 2020; 111(5-6): 1587-1602.
15. Wang CY, Xie YX, Zheng LJ, et al. Research on the chip formation mechanism during the high-speed milling of hardened steel. *International Journal of Machine Tools & Manufacture* 2014; 79: 31-48.
16. Denkena B, Köhler J. Consideration of the form of the undeformed section of cut in the calculation of machining forces. *Machining Science and Technology* 2010; 14(4): 455-470.
17. Ding F, Wang CY, Zhang T, et al. Investigation on chip deformation behaviors of Zr-based bulk metallic glass during machining. *Journal of Materials Processing Technology* 2020; 276:116404.
18. Jiang MQ, Dai LH. Formation mechanism of lamellar chips during machining of bulk metallic glass. *Acta Materialia* 2009; 57(9): 2730-2738.
19. Dhale K, Banerjee N, Singh RK, et al. Investigation on chip formation and surface morphology in orthogonal machining of Zr-based bulk metallic glass. *Manufacturing Letters* 2019; 19: 25-28.
20. Chau SY, To S, Sun ZW, et al. Twinned-serrated chip formation with minor shear bands in ultra-precision micro-cutting of bulk metallic glass. *International Journal of Advanced Manufacturing Technology* 2020; 107(11-12): 4437-4448.
21. Avila KE, Vardanyan VH, Urbassek HM. Transition to chip serration in simulated cutting of metallic glasses. *European Physical Journal B* 2021; 94(7):152.
22. Chen X, Xiao JF, Zhu Y, et al. Micro-machinability of bulk metallic glass in ultra-precision cutting. *Materials & Design* 2017; 136: 1-12.
23. Wang B, Liu Z, Yang Q. Chip formation characteristics in high-speed machining of hardened AIS11045 steel. *Advanced Materials Research* 2012; 565: 484-489.
24. Tang HH, Meng L, Zhang JC, et al. On the fractal analysis of the serration behavior of a bulk metallic glass composite. *Journal of Alloys and Compounds* 2022; 895:162605.